

A prototype coded aperture imaging- based radiation localization and identification system

Tushar A Kesarkar, Sourav Mukhopadhyay,
Menka Sukhwani, PV Bhatnagar
Electronics Division, BARC



Contents

- Gamma Imager: Radiation localization and identification system (RLIS)
- Coded aperture imaging (CAI)
- MURA mask-based CAI
- Various detector technologies for CAI-RLIS
- Physics simulation and proof of concept
- A prototype RLIS system development
 - ✓ Pixelated detector
 - ✓ MURA mask
 - ✓ precision mechanical assembly
 - ✓ Image reconstruction and interactive GUI
- Results and discussion
- Conclusion and future scope

Gamma Imager: Radiation localization and identification (RLIS) system

- Gamma rays are highly penetrating and cannot be focused by traditional lenses
- Locate and identify gamma ray sources by combining directional imaging with spectroscopy.

Popular Approaches

Compton imaging

Raster scanning

Mechanical collimation

Coded-aperture imaging

Hybrid methods

Salient features

Angular resolution ($\Delta\theta$)

Field of view (FoV)

Energy resolution

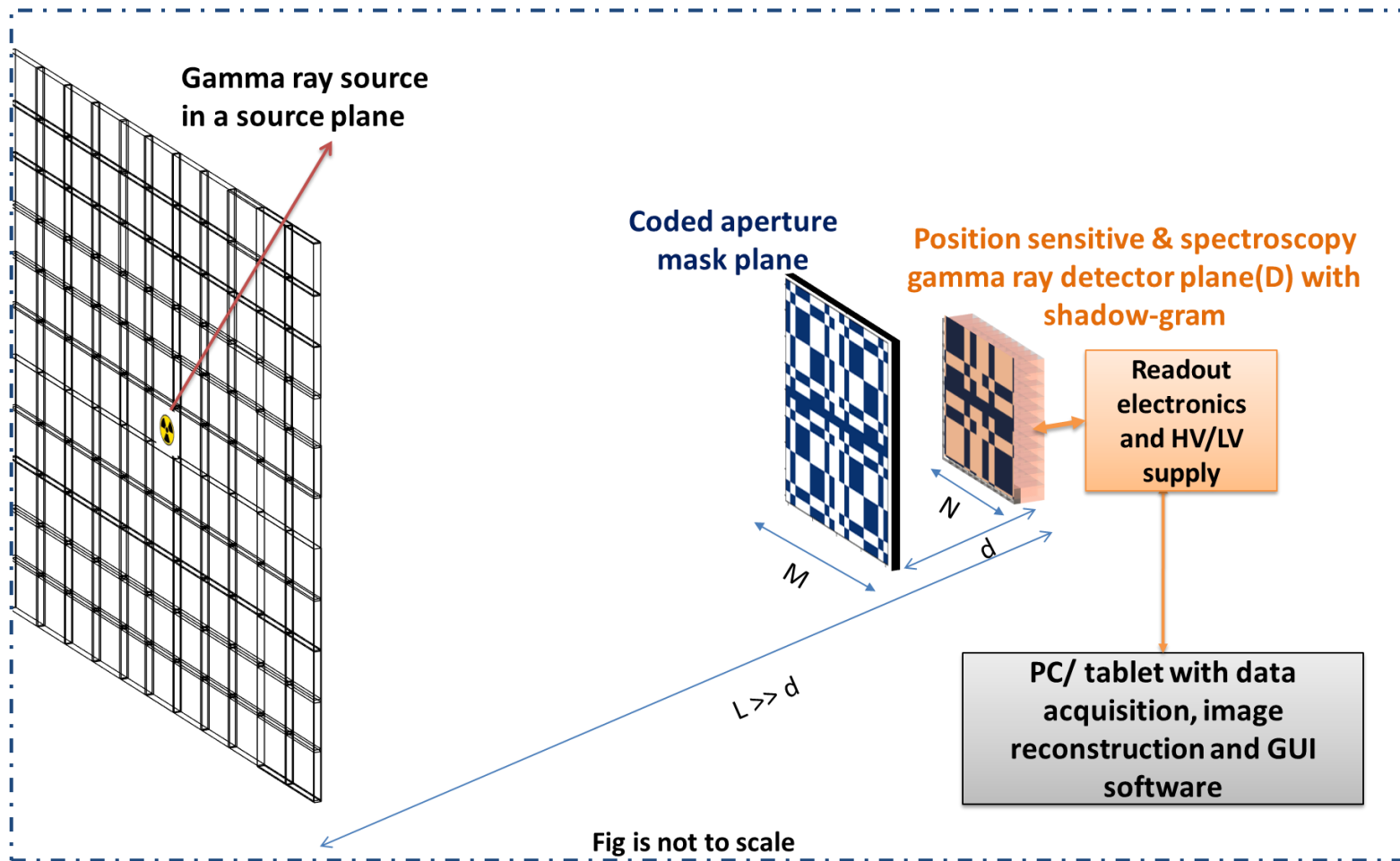
Dose rate and response time

Spectrometer Range (keV)

➤ Applications:

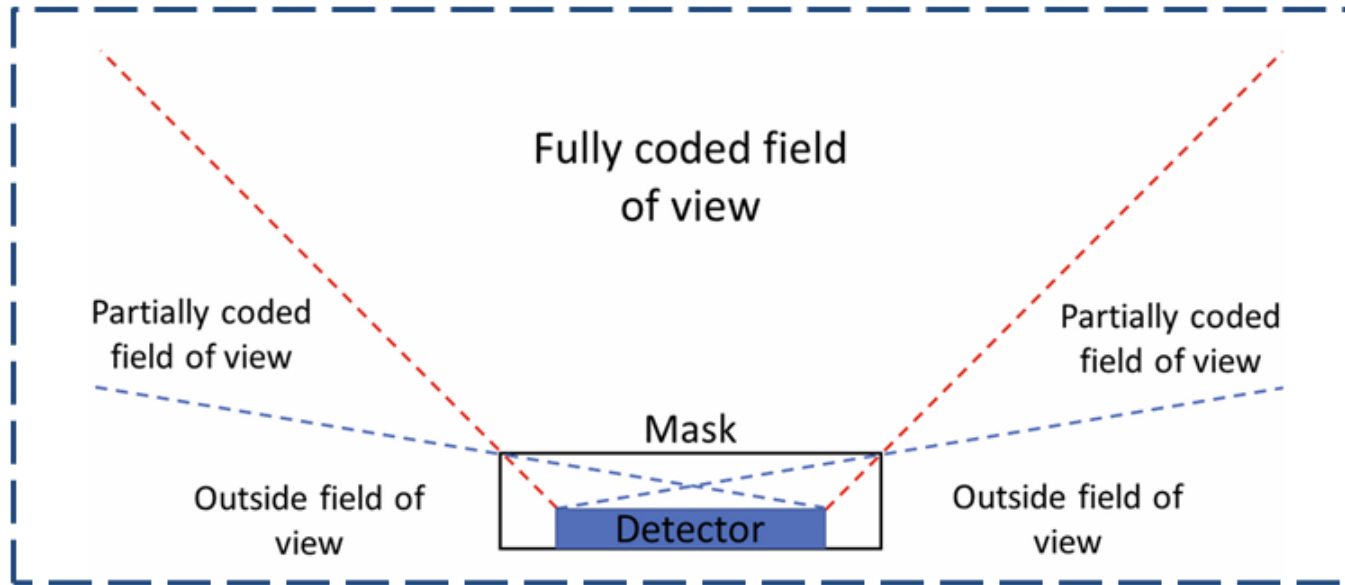
- Homeland security
- Emergency radiation response
- Nuclear decommissioning & waste management
- Medical imaging (SPECT)

Coded Aperture Imaging (CAI)–based gamma RLIS



Typical CAI based RLIS setup showing source plane (S), coded aperture mask plane (A), and detector plane (D) with image reconstruction software

Figure of Merit (FoM)



Fully coded field of view (FCFOV),

$$\theta_{FC} = 2 \tan^{-1} \left(\frac{(M - N)/2}{d} \right)$$

L : Source - detector plane distance

d: Mask - detector plane distance (focal length)

M: Mask dimension

N: Detector dimension

Partially coded field of view (PCFOV),

$$\theta_{PC} = 2 \tan^{-1} \left(\frac{M/2}{d} \right)$$

The shadow-gram on the detector is fully coded through mask or partially

Angular resolution,

$$\Delta\theta \approx \frac{p}{d}$$

P is the smallest aperture hole dimension

The Basics

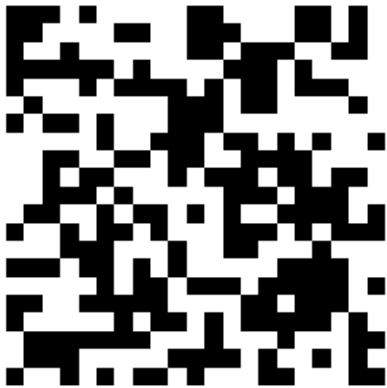
- Mathematically, the data recorded by the detector (D) is the convolution of the source distribution (S) and the mask aperture function (A), plus background noise (N)

$$D = S * A + N$$

- To recover the source image (\hat{S}) we correlate the detector data with a decoding mask (G)

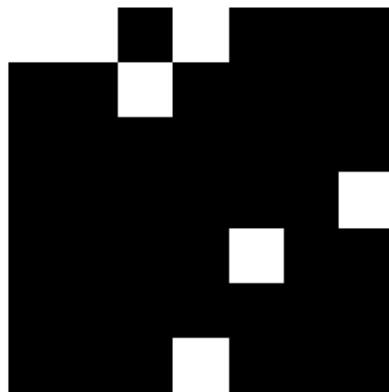
$$\hat{S} = D * G + N * G$$

- Various types of coded masks, made of high Z material like Tungsten, are used for gamma ray imaging applications

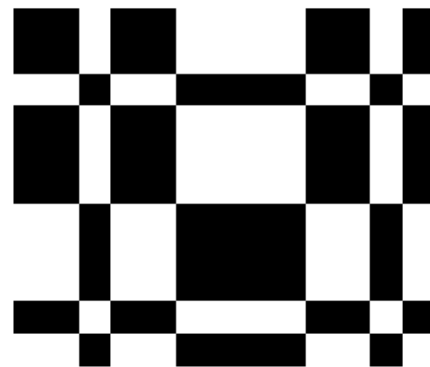


Random mask

03/02/2026

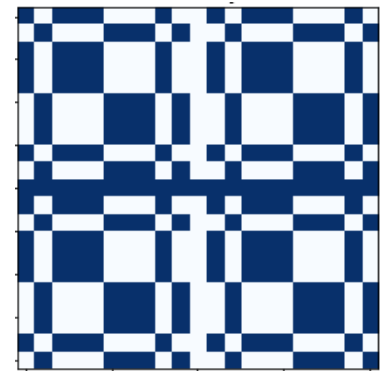


Non redundant array



Uniformly redundant array
(URA)

TIPP 2026



2x2 Mosaic of
Modified URA₆

MURA mask-based CAI

Features	NRA mask [1]	Random Mask[1]	URA[1]	MURA[2]
Transparency/ Sensitivity	Very Low (<10%)	Adjustable (often 50%)	High (50%)	High (50%)
Autocorrelation	Delta + Flat Side-lobes	Noisy with side lobes artifacts	Perfect Delta	Perfect Delta
Ideal Geometry	Any	Any	Rectangular (P×P+2)	Square (P×P)

- ❖ MURA mask aperture **A** is chosen such that its periodic correlation with the decoding aperture **G** (same as A except central element) is a delta function (δ):

$$\mathbf{A} * \mathbf{G} = \delta$$

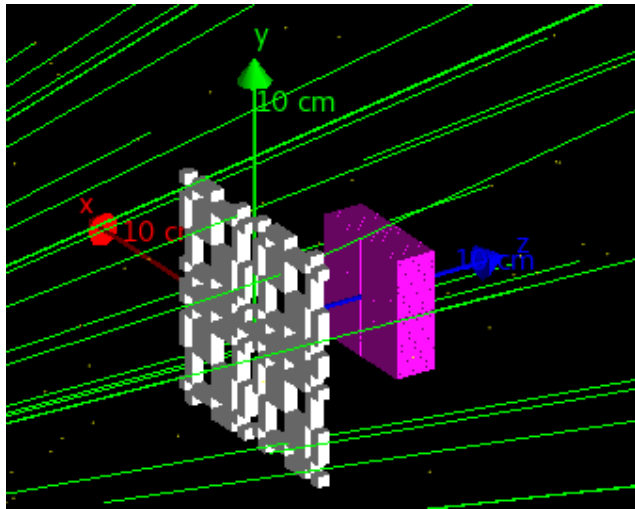
- ❖ In ideal case, perfect localization **no side lobes and other artifacts** [2]
- ❖ The **transparency** (open fraction) is $\sim 50\%$, maximizing the **sensitivity and Signal-to-Noise Ratio (SNR)**
- ❖ The aperture (**A**) is made from **2x2 mosaic** of basic MURA pattern by cyclic repetition. This allows for **wide FoV** imaging with **small detector size** [1].
- ❖ MURA mask is **anti-symmetric** -> **anti-mask** by rotating the mask by 90 degrees-> **Non uniform background correction and SNR improvement.**

Detector technologies for CAI-RLIS

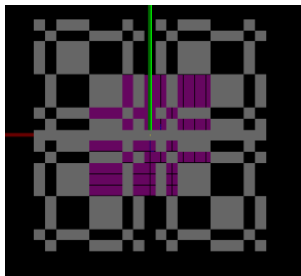
Pixelated Detector technology	Energy resolution	Spatial granularity	Key Features
Scintillators + Multi anode PMT (NaI(Tl), CsI(Tl), BGO) [3,4]	~ 6–12% @662 keV	mm–cm (light sharing limits finest pitch)	Large-area , high stopping power, low cost; limitation: poor energy resolution ; hygroscopic (NaI) and bulky with PMTs, PMT affected by magnetic field
Pixelated scintillators + SiPM (LaBr3(Ce), CsI(Tl), CLLB) [4,5]	~ 2.5–7% @662 keV	mm	Better energy and spatial resolution; MRI-compatible, fast timing, compact limitation: higher cost, intrinsic background, gain variations, requires SiPM ASIC & temperature control .
CZT semiconductor [6,7]	~1–3% @662 keV	sub - few mm	Excellent energy & spatial resolution & 3D position using DOI correction, ideal for RLIS limitation: very high cost , complex electronics

[3] Milbrath et al., Appl. Opt., 2005.[4] Derenzo et al., NIM A, 2002.[5] Gola et al., NIM A, 2019.
[6] Barber, NIM A, 1999.[7] Hong et al., NIM A, 2007.

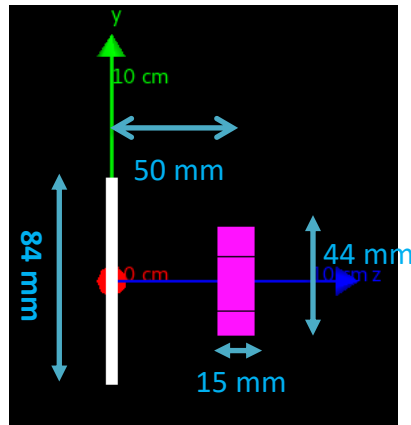
Physics simulation and proof of concept



Oblique view of the detector, mask and source plane



Front view



Sketch of the simulation setup

Geant4 simulation setup showing 5mm thick mosaic Rank-11 MURA mask (Grey) and pixelated CZT detector (pink)

- **Geant4 Monte-Carlo modeling** of the RLIS system
- Realistic **mask-detector – source geometry** including **finite mask and pixelated detector thickness, mask-detector spacing**, and source positions spanning FCFOV
- W–Ni (90:10) alloy MURA mask modeled with accurate material attenuation to simulate gamma ray **transmission, self-collimation** effects
- Multiple γ -ray sources simulated with controlled energy, activity
- Combination of **Mask-anti-mask [8]** configurations used to reduce background, detector non-uniformity, and systematic artifacts.
- **Image reconstruction algorithms** are optimized based on simulation results

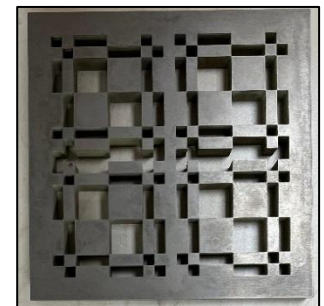
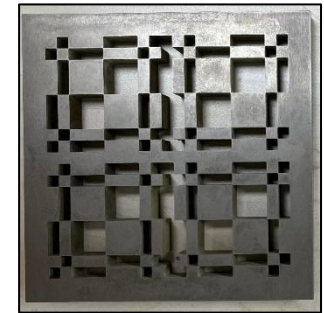
Development of a prototype CAI based RLIS system

Commercial Pixelated detector module specifications

Parameter	Specifications
Material / Type	Pixelated CZT
Pixel matrix	22 × 22 (484 pixels)
Active area / Thickness	44 × 44 mm ² / 15 mm
Pixel size	2 × 2 mm ²
Energy resolution & Readout	< 3 % @ 662 keV; per-pixel CSA + 4k ADC

Coded aperture MURA mask specifications

Parameter	Specifications
Mask type	2×2 mosaic of Rank-11 MURA (21 × 21)
Overall dimension	100 × 100 mm ²
Thickness options	5 mm / 10 mm
Smallest hole size	4 mm
Material & features	W–Ni alloy (W > 90%); self-supporting, stackable 90° rotatable anti-mask



Fabricated W-Ni alloy based rank-11 MURA mask and anti-mask (rotated by 90 degree)

Development of a prototype CAI based RLIS system

Precision mechanical assembly

- **Material:** Low-Z **nylon** to minimize gamma attenuation and scattering.
- **Micro-meter-based X–Y alignment** of coded aperture mask relative to the detector with **< 100 μm accuracy**.
- **Adjustable aperture–detector separation (d)** using interchangeable **nylon spacers** for various experimental test setups
- Easy **stacking and rotating** of coded masks
- **Acrylic stand and grid-based source plane** with precise source to detector distance (L) in **Z-direction** for **quantitative evaluation of localization performance**.

Development of a prototype CAI based RLIS system

Image Reconstruction algorithms

➤ **Balanced Correlation (BC)**

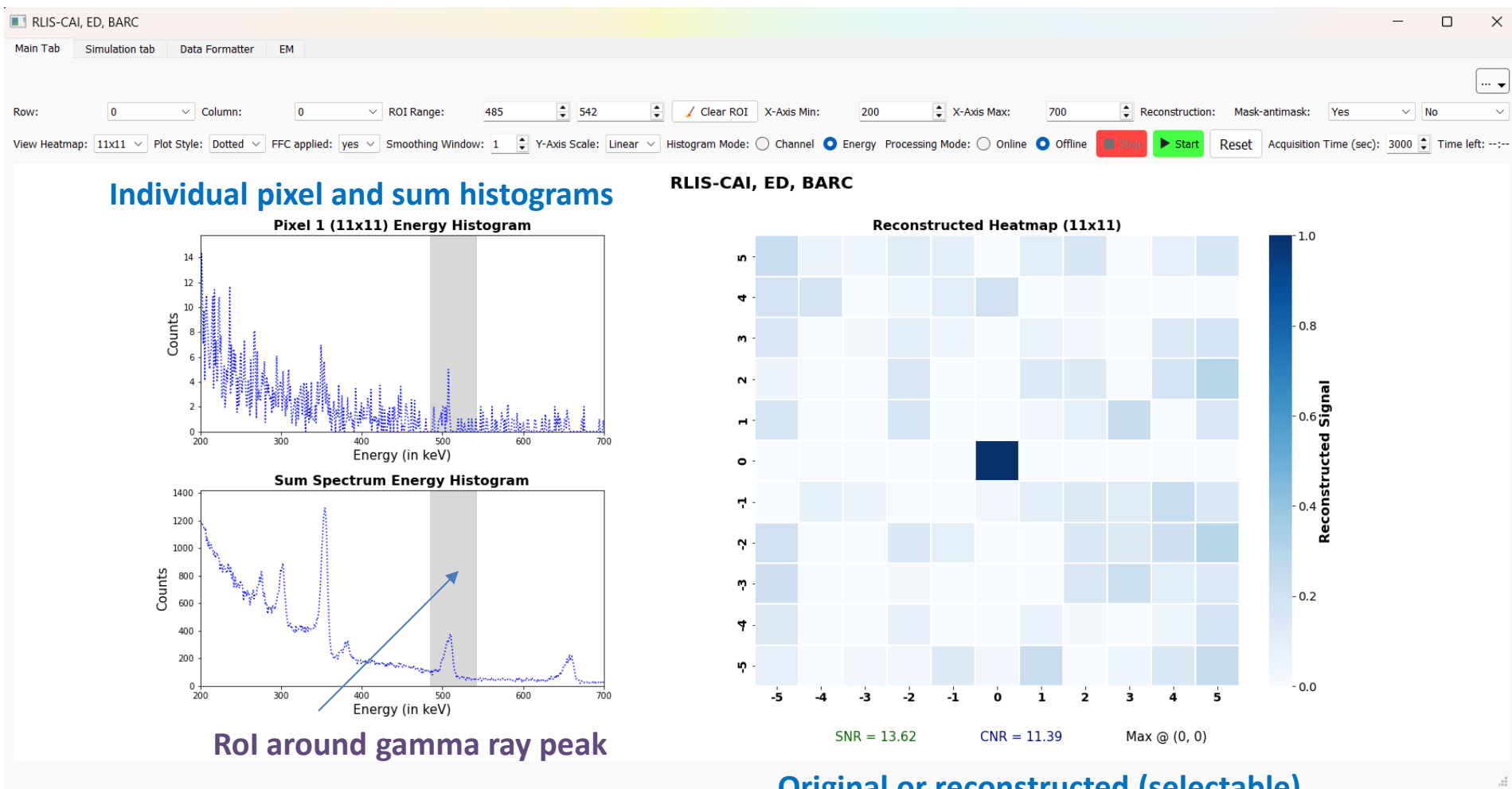
- Image reconstruction by correlating the detector data with **decoding mask**
- Assumes **shift-invariant response** and far-field geometry
- **Single-step and computationally fast**
- Performance degrades in low-count, **non-uniform background conditions** -> can be improved with **mask-anti-mask technique**

➤ **Maximum Likelihood Expectation Maximization (MLEM) [9]**

- **Statistical reconstruction** method
- Detector counts modelled using **Poisson statistics**
- **System matrix** incorporating mask and geometry
- Image estimate is **iteratively refined** using **forward and back projection**
- Enforces non-negativity and statistical consistency of the solution
- **High-contrast** images with suppressed artifacts and accurate multi-source localization

Development of a prototype CAI based RLIS system

Interactive GUI

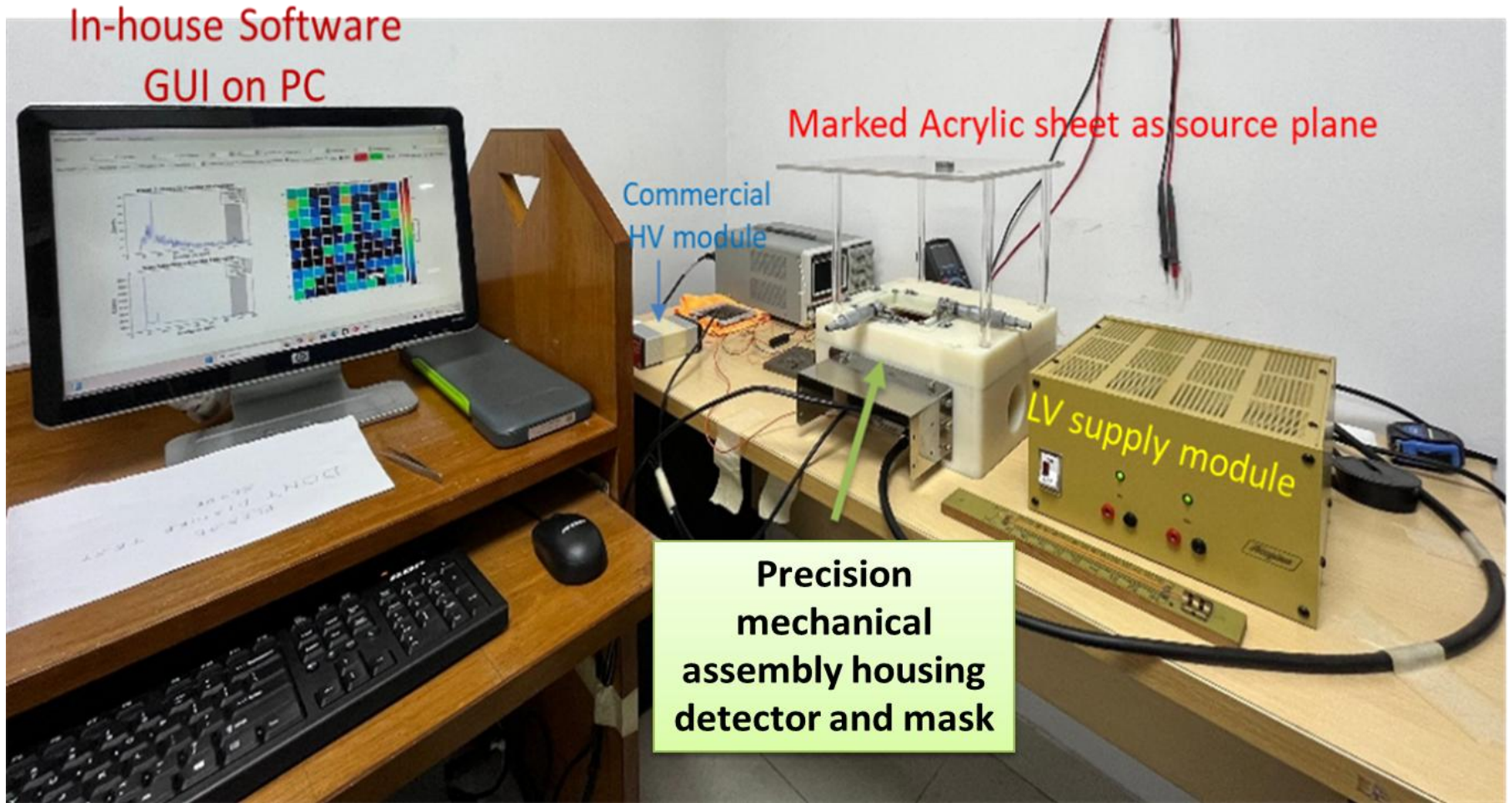


RoI around gamma ray peak

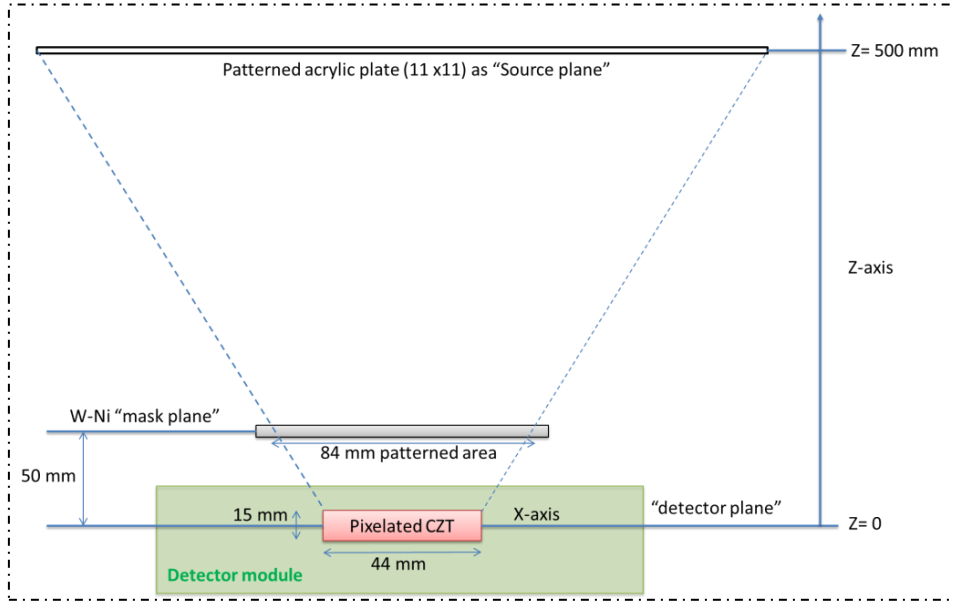
Original or reconstructed (selectable)
Heat map (energy windowed)

- Main tab and simulation tab
- Image reconstruction

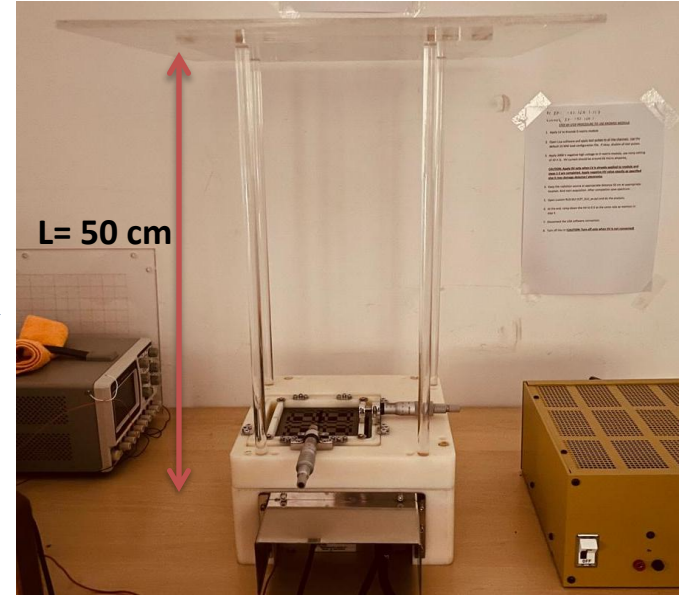
The prototype CAI-RLIS



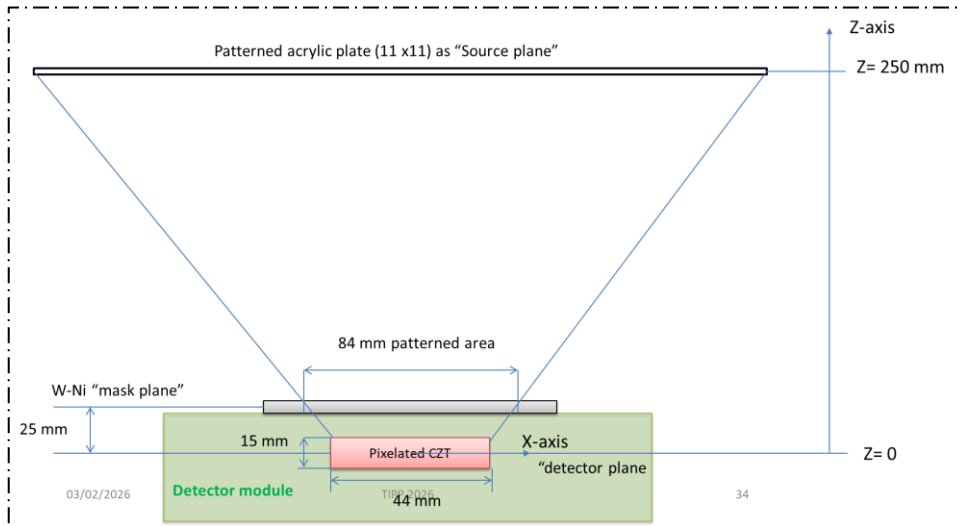
Experimental Test Setups



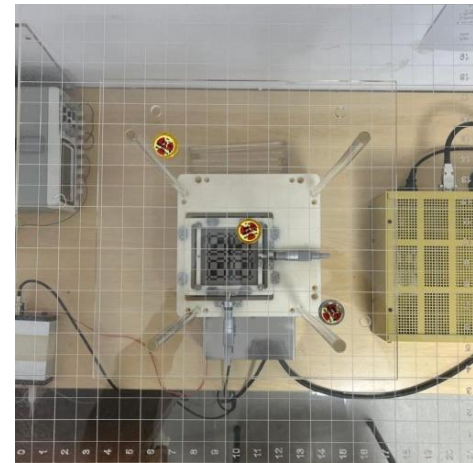
Test setup 1



Front-view of the Test setup 1



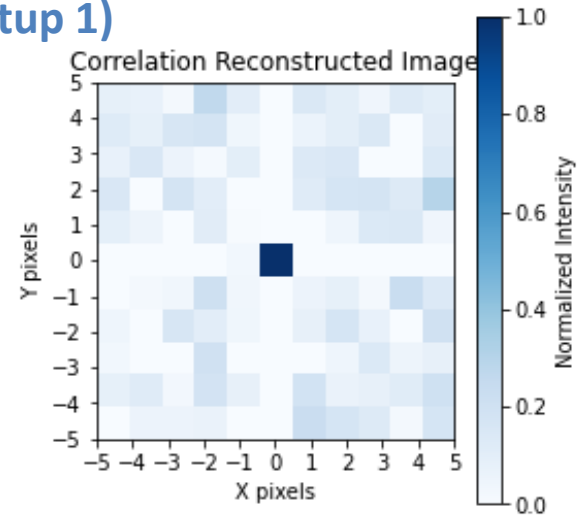
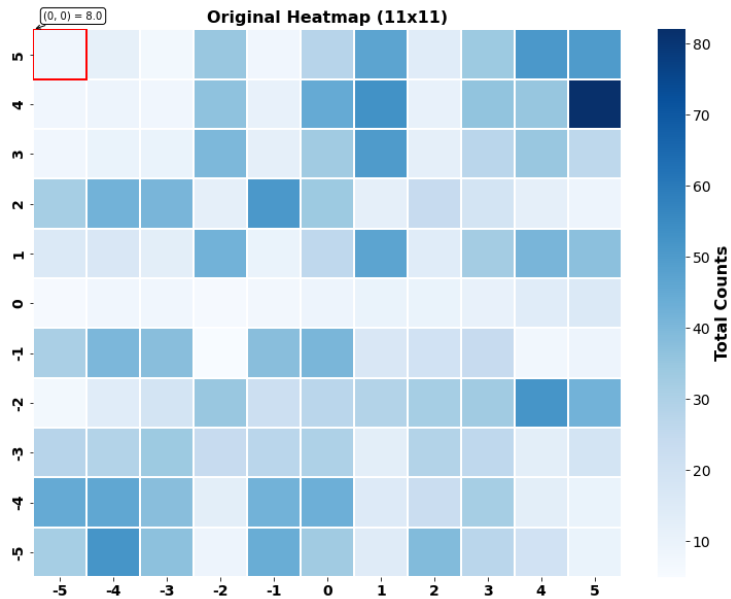
Test setup 2



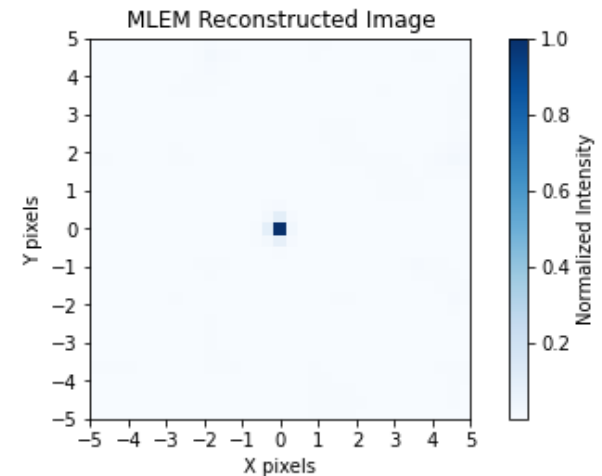
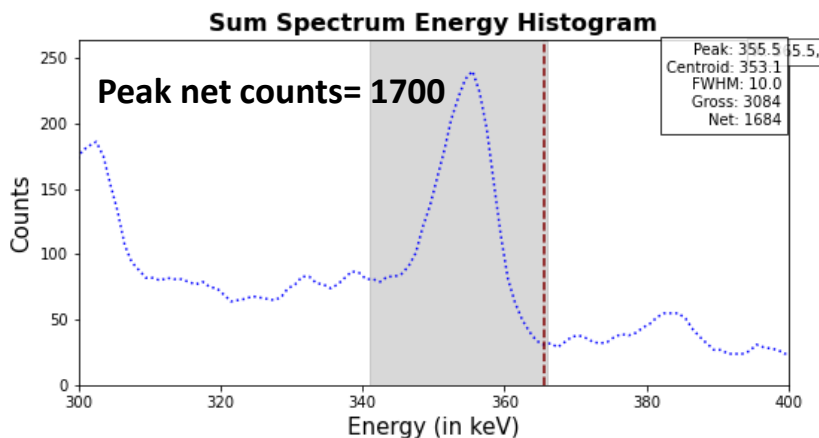
Top view of the "source plane"

Results and Discussions

- Test Case 1: Ba-133 (100 kBq) source at (0,0)
- Acquisition time= 20 mins, d= 50 mm, L= 50 cm (Setup 1)



SNR = 9.09 | CNR = 49.72 | max@(0.00, 0.00)

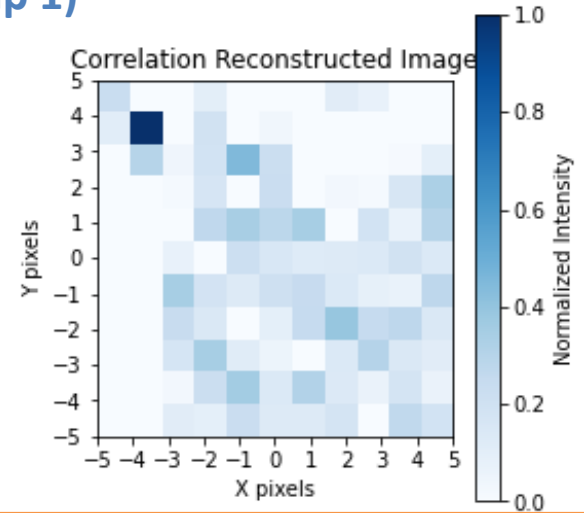
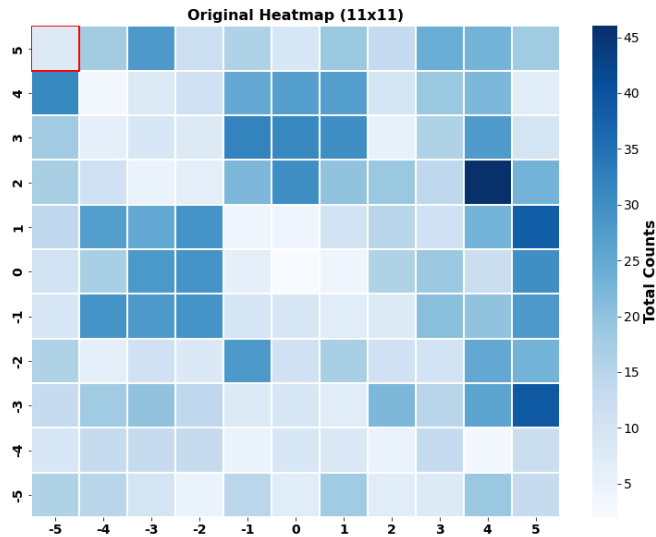


SNR = 32.65 | CNR = 26.67 | max@(0.00, 0.00)

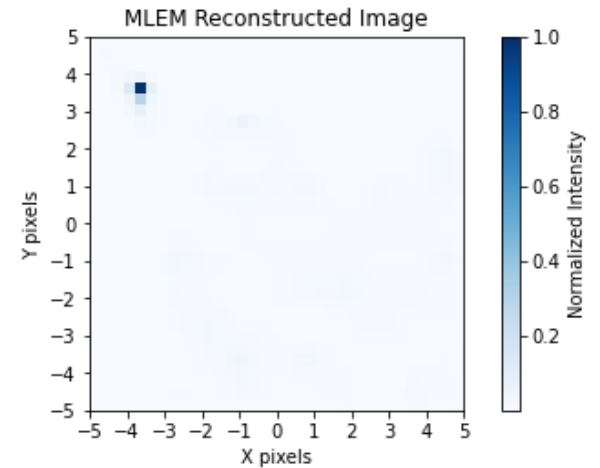
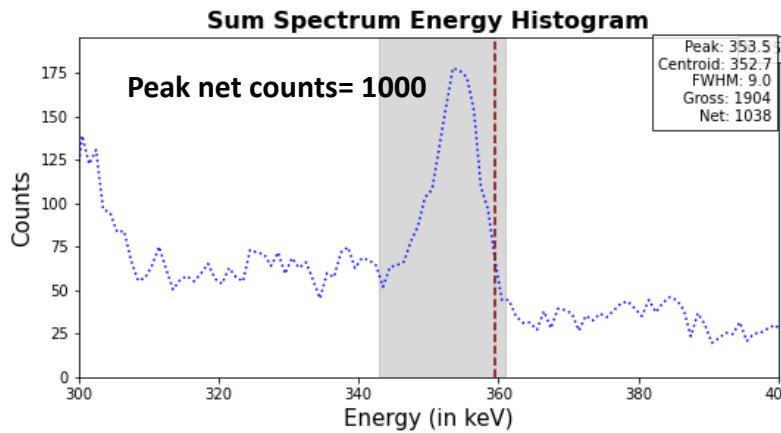
MLEM improves the reconstructed image quality

Results and Discussions

- Test case 1 : Ba-133 (100 kBq) source at (-4,4)
- Acquisition time= 20 mins, d= 50 mm, L= 50 cm (Setup 1)



SNR = 7.12 | CNR = 8.19 | max @ (-4.00, 4.00)

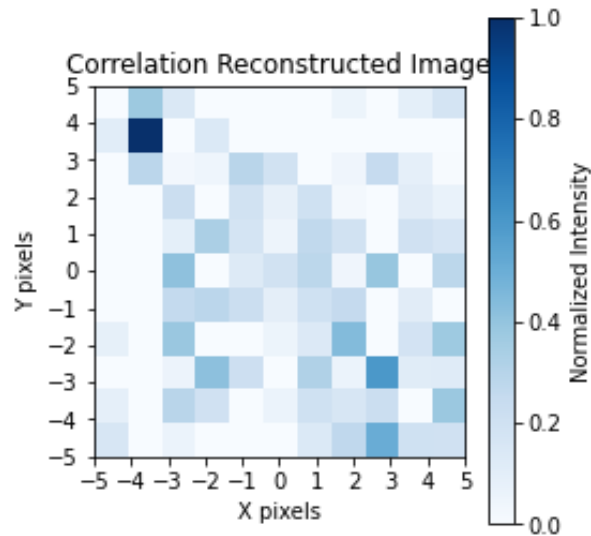


SNR = 30.98 | CNR = 10.60 | max @ (-3.75, 3.75)

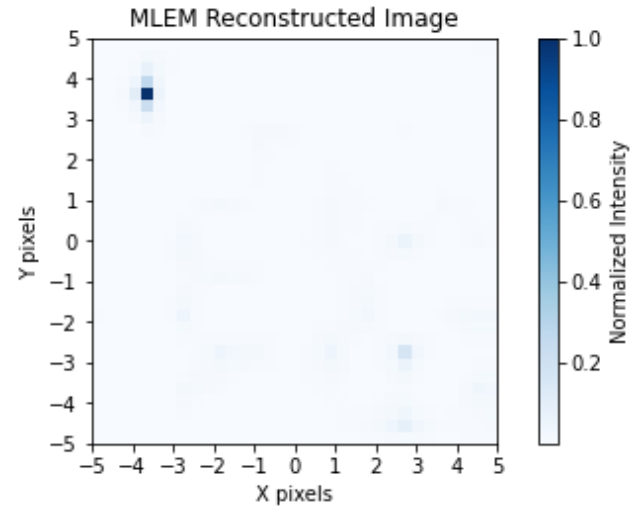
Image reconstruction is best at the center of the FCOV
due to larger net counts as compared to periphery

Results and Discussions

- Test case 2: Cs-137 (50 kBq) source at (-4,4)
- Acquisition time= 40 mins, d= 50 mm, L= 50 cm (Setup 1)



SNR = 6.39 | CNR = 6.55 | max @ (-4.00, 4.00)



SNR = 30.16 | CNR = 10.14 | max @ (-3.75, 3.75)

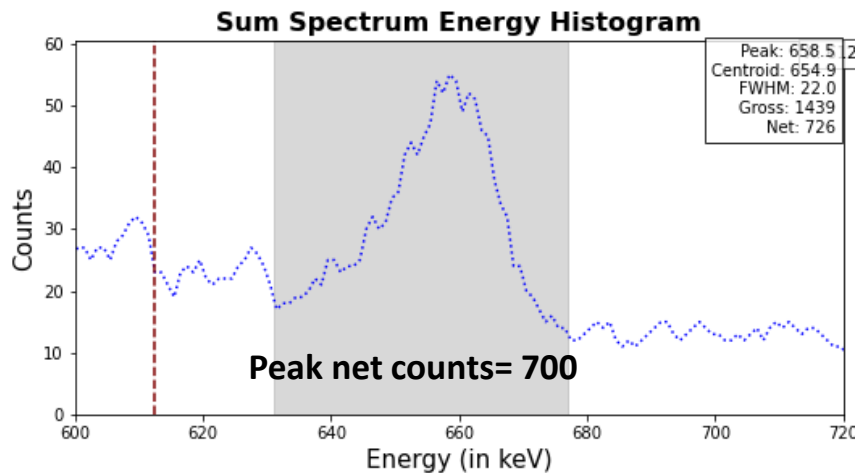


Image reconstruction superior for Ba-133 as compared to Cs-137 source due to larger net counts

Results and Discussions

Test case 3: Cs-137 (50 kBq) source at (0,0) d= 25 mm, L= 25 cm Acquisition time= 15 mins (setup2)

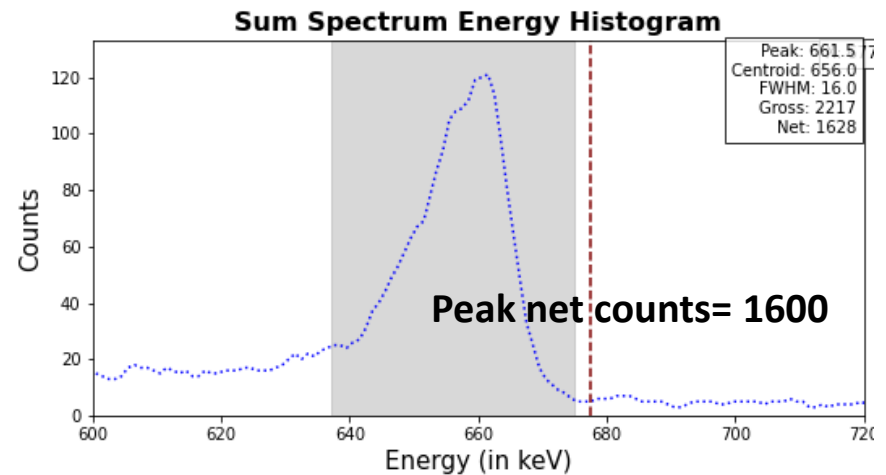
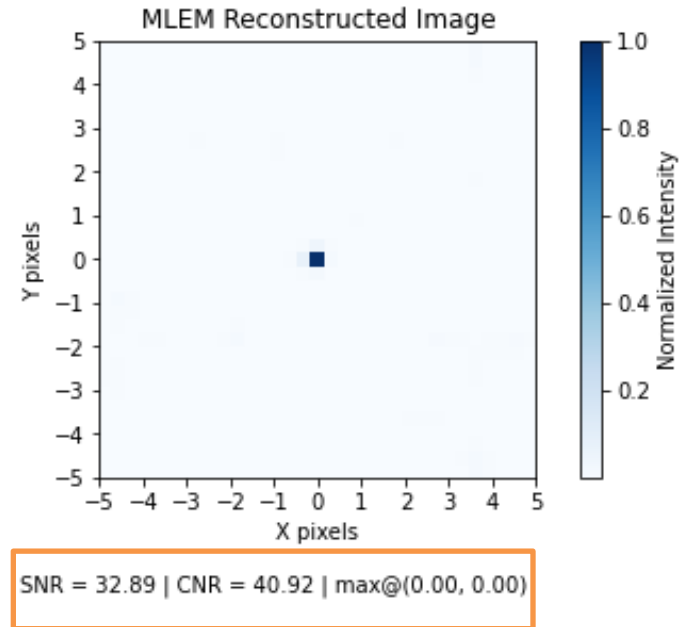
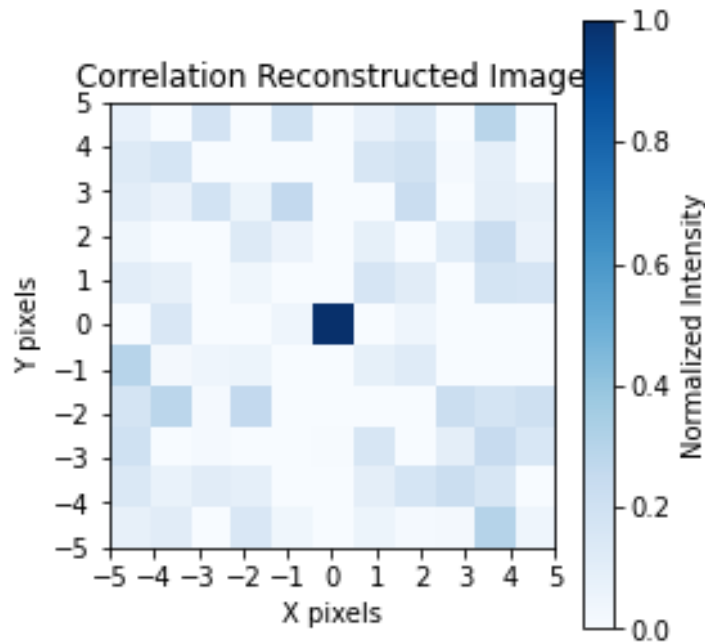
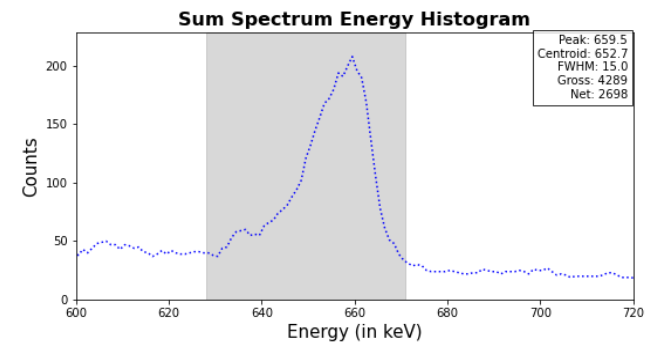
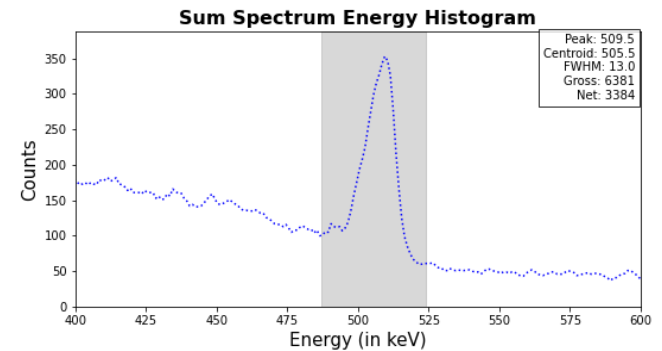
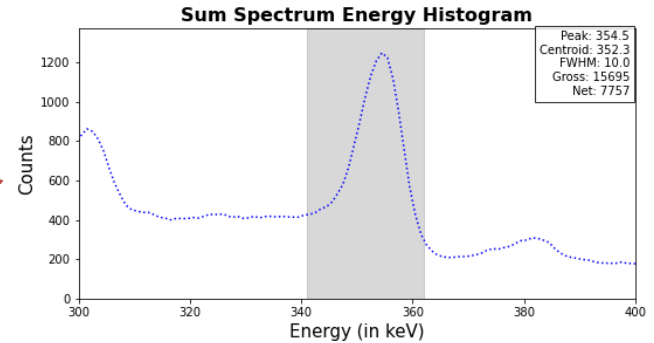
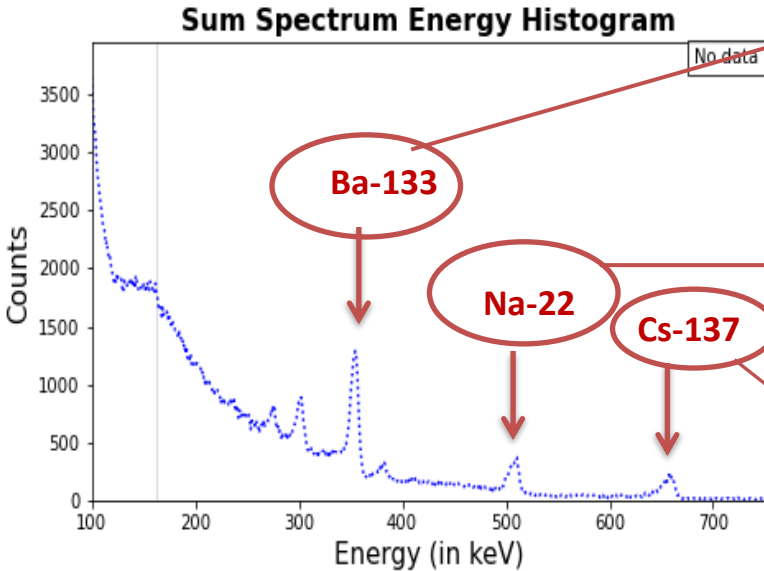


Image reconstruction faster with nearer source plane

Results and Discussions: Test case 4 (multi-source case)

Three lab sources Ba-133 (100 kBq), Na-22 (12 kBq) & Cs-137 (50 kBq)

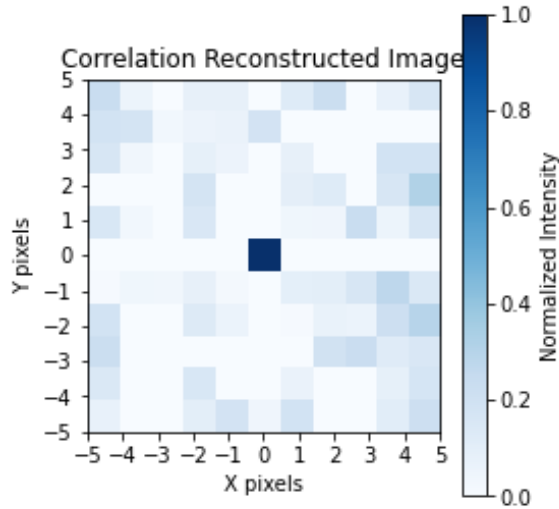
Acquisition time= 30 mins, d= 25 mm, L= 25 cm (setup 2)



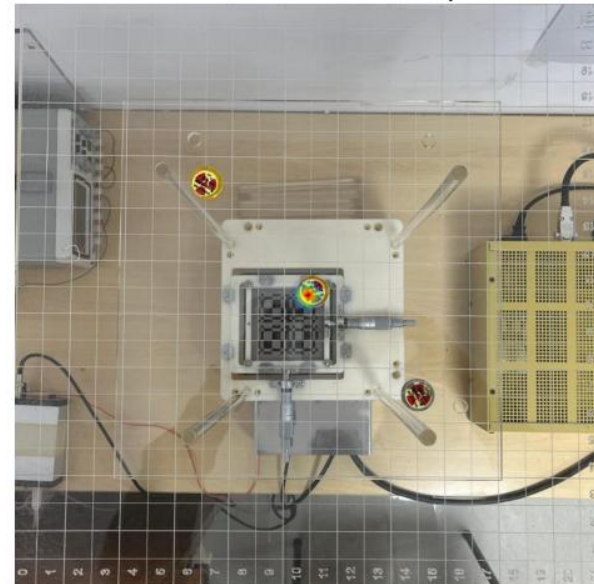
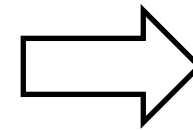
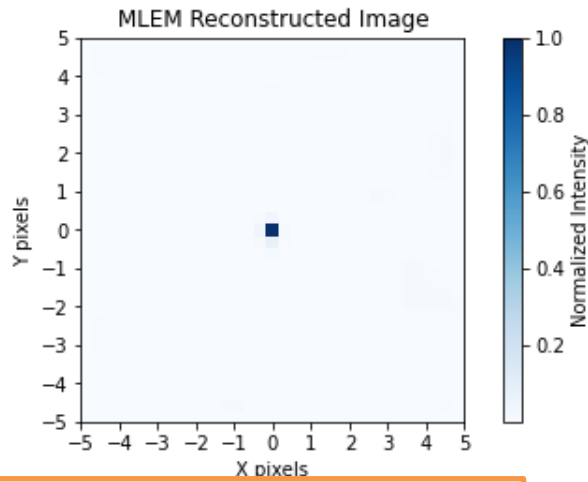
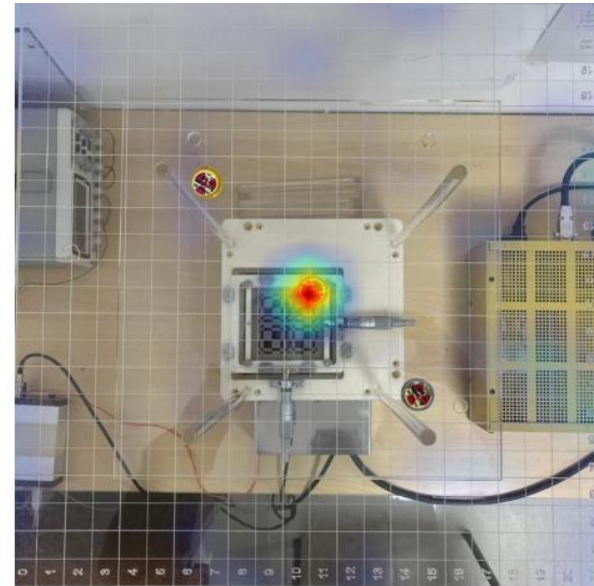
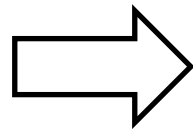
Gamma Energy (keV)	Radioisotope	Energy Resolution (% FWHM)
356	Ba-133	2.8 %
511	Na-22	2.5 %
662	Cs-137	2.2 %

Results and Discussions: Test case 4 (multi-source case)

Na-22 source at 0,0 energy window (Setup 2)



SNR = 8.49 | CNR = 32.62 | max@(0.00, 0.00)

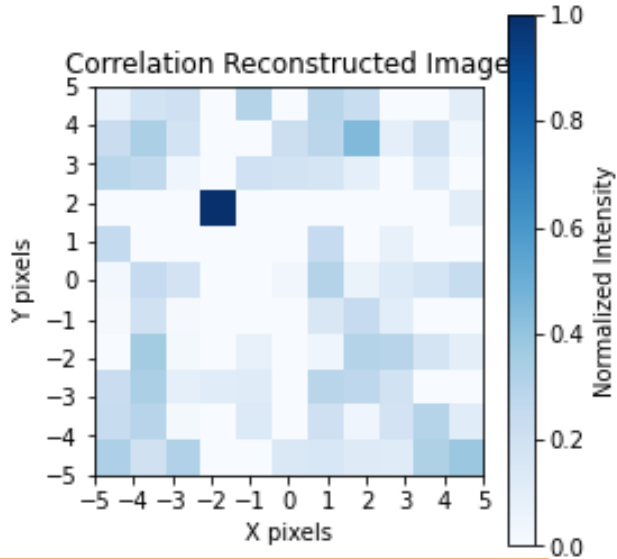


Peak net counts = 3300

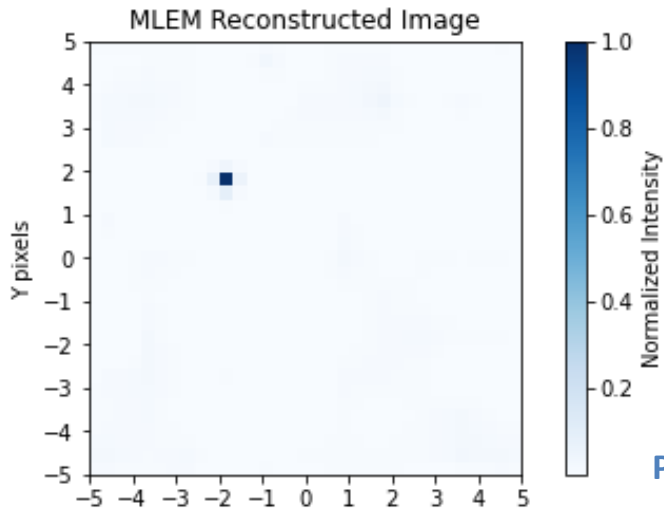
Gamma Image superimposed on optical image

Results and Discussions: Test case 4 (multi-source case)

Cs-137 source at -2,2 energy window (Setup 2)

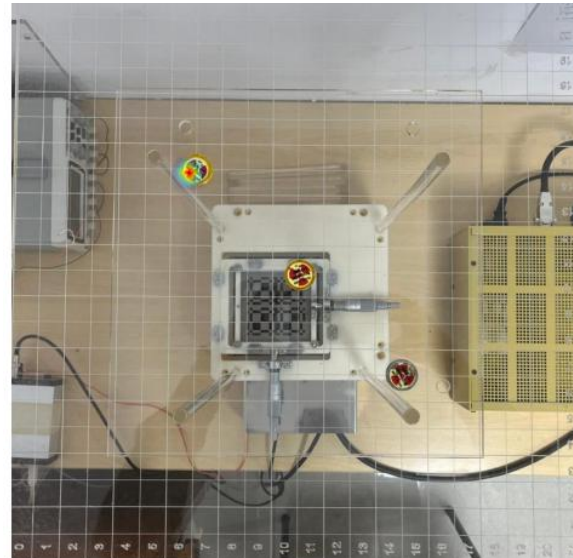
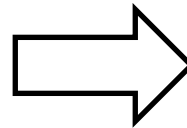
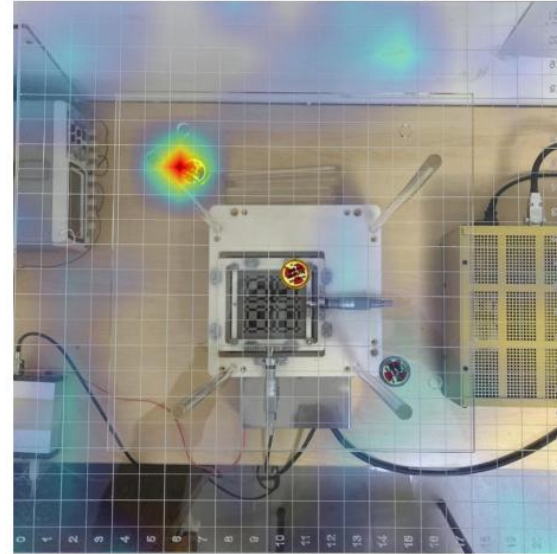
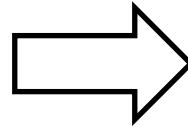


SNR = 6.95 | CNR = 14.69 | max @ (-2.00, 2.00)



SNR = 32.57 | CNR = 32.68 | max @ (-1.88, 1.88)

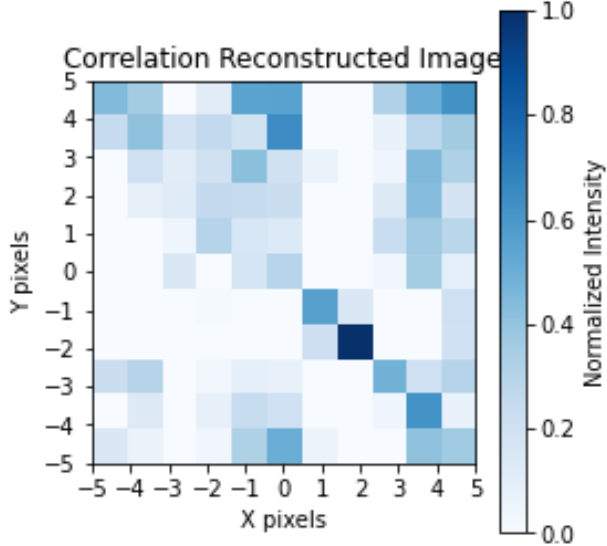
Peak net counts = 2600



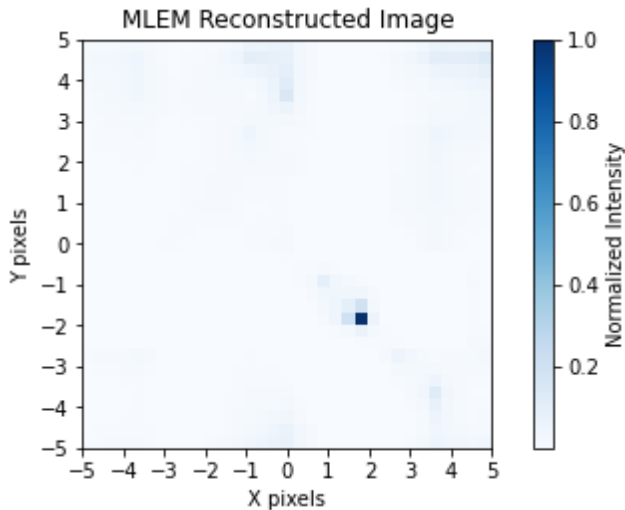
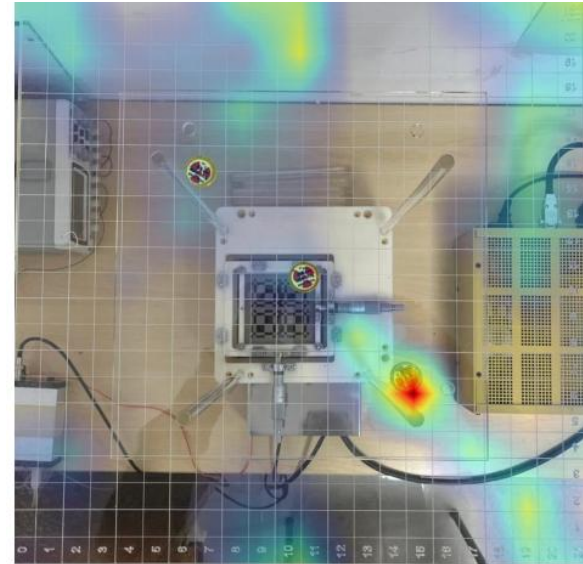
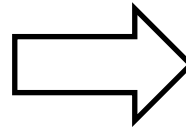
Gamma Image superimposed on optical image

Results and Discussions: Test case 4 (multi-source case)

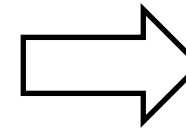
Ba-133 source at 2,-2 energy window (Setup 2)



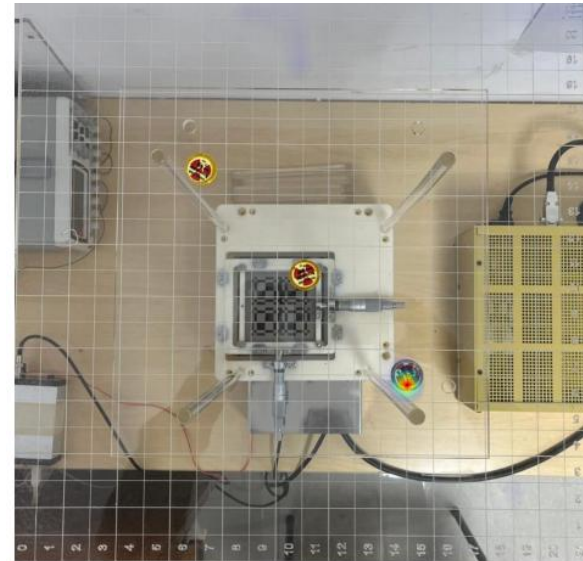
SNR = 5.26 | CNR = 3.86 | max @ (2.00, -2.00)



SNR = 28.44 | CNR = 12.89 | max @ (1.88, -1.88)



Peak net counts = 7700



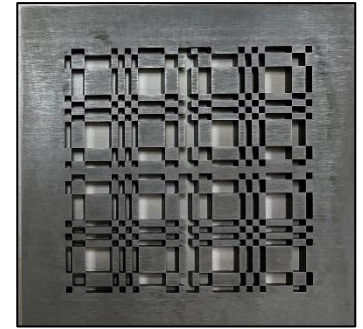
Gamma Image superimposed on optical image

Summary of Outcomes

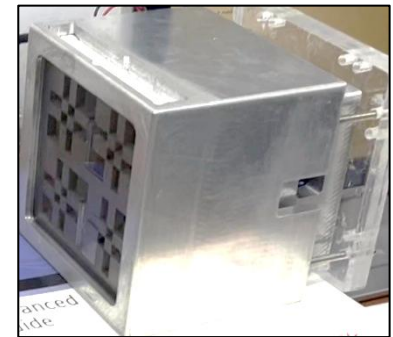
Test case & setup	Mask Thickness (t)	Radioactive Source & Position	Acquisition Time for high CNR	Angular resolution & FoV	Remarks
Test case 1 setup 1 d= 50 mm L= 50 cm	5 mm	Ba-133 (100 kBq), single lab source within FCFOV	20 min	4.6 deg with FCFOV = 44 deg	Source could be clearly localized using RoI around 356 keV photo-peak
Test case 2 setup 1 d= 50 mm L= 50 cm	5 mm	Cs-137 (50 kBq), single lab source within FCFOV	40 min	4.6 deg FCFOV = 44 deg	Source could be clearly localized using RoI around 662 keV photo-peak
Test case 3 setup2 d= 25 mm L= 25 cm	5 mm	Cs-137 (50 kBq), single lab source within FCFOV	15 min	9.2 deg FCFOV = 44 deg	Source could be clearly localized using RoI around 662 keV photo-peak
Test case 4 setup2 d= 25 mm L= 25 cm	5 mm	Ba-133 (100kBq), Cs-137 (50kBq) and Na-22 (12 kBq), three lab source within FCFOV	30 min	9.2 deg with FCFOV = 44 deg	Source could be clearly localized using RoI around 356 keV, 661 keV and 511 keV photo-peaks

Conclusion and Future work

- A prototype radiation localization and identification system (RLIS) using coded aperture imaging (CAI) technique has been developed.
- The RLIS system performance has been optimized using Geant4 based simulation and characterized in lab for gamma ray imaging.
- The RLIS system is tested for angular resolution of 4.6 deg with high CNR over a field of view of 44 deg for gamma ray lab sources over detector energy range. The measured energy resolution is 2.2 % at 662 keV.
- Though the system is tested for far-field source configuration, it can be tuned to near field applications.
- The system response time vs dose rate performance needs to be evaluated in detail for various gamma ray energies.
- Rank-19 MURA mask with 2mm aperture is fabricated and will be tested.
- Compton and hybrid imaging techniques will be implemented to achieve wider FoV.
- Development of hand held CAI-RLIS instrument will be initiated.



100 mm x 100 mm Rank-19 MURA patterned mask



Compact RLIS system under development

References

1. E. E. Fenimore & T. M. Cannon — Coded aperture imaging with uniformly redundant arrays. *Appl. Opt.* 17, 337–347 (1978).
2. S. R. Gottesman & E. E. Fenimore — New family of binary arrays for coded aperture imaging. *Appl. Opt.* 28, 4344–4352 (1989)
3. B. D. Milbrath et al., “Comparison of LaBr₃:Ce and NaI(Tl) scintillators for radioisotope identification,” *Appl. Opt.*, vol. 44, pp. 2977–2984, 2005.
4. S. E. Derenzo et al., “Scintillation properties of NaI(Tl), CsI(Tl), BGO, and LaBr₃(Ce),” *Nucl. Instrum. Methods Phys. Res. A*, vol. 486, pp. 214–219, 2002.
5. A. Gola et al., “Silicon photomultiplier technology for gamma-ray detection and imaging,” *Nucl. Instrum. Methods Phys. Res. A*, vol. 926, pp. 106–120, 2019.
6. H. B. Barber, “Applications of semiconductor detectors to nuclear medicine,” *Nucl. Instrum. Methods Phys. Res. A*, vol. 436, pp. 102–110, 1999.
7. J. Hong et al., “Laboratory coded-aperture imaging using depth-sensitive CZT detectors,” *Nucl. Instrum. Methods Phys. Res. A*, vol. 573, pp. 122–126, 2007.
8. Cieślak, M. J., Gamage, K. A. A., & Glover, R. (2016). Coded-aperture imaging systems: Past, present and future development – A review. *Radiation Measurements*, 92, 59-71. <https://doi.org/10.1016/j.radmeas.2016.08.002>
9. A. J. Accorsi, F. Gasparini, and R. Lanza, “Coded aperture imaging in nuclear medicine,” *Nucl. Instrum. Methods Phys. Res. A*, vol. 580, pp. 1311–1322, 2007.

Acknowledgements

- We are grateful to Dr. V. B. Chandratre, Ex-Head, Microelectronics Section, ED, BARC for his guidance, support and motivation.
- We are thankful to our colleagues at Microelectronics Section, ED, BARC and Head, ED, BARC for their support and encouragement.
- We also would like to thank our vendors for fabrication of precision mechanical assembly and coded aperture masks.
- We would also like to acknowledge the contributions of the project trainees Ms. Neerjakshi Chimurkar, Ms. Nivedita P. Hari and Ms. Srijani Pahari in the development of the user interface.

THANK YOU